Dalton Transactions

PAPER

View Article Online
View Journal | View Issue

Cite this: *Dalton Trans.*, 2017, **46**, 11201

Ligand-directed synthesis of $\{Mn^{III}_5\}$ twisted bow-ties†

María José Heras Ojea, [a] Moya A. Hay, [a] Giacomo Cioncoloni,[a] Gavin A. Craig, ‡[a] Claire Wilson, [a] Takuya Shiga,[b] Hiroki Oshio, [b] Mark D. Symes [a] and Mark Murrie *[a]

Received 5th July 2017,
Accepted 24th July 2017

DOI: 10.1039/c7dt02430d

rsc.li/dalton

Two isostructural polymetallic complexes $[Mn^{III}_5(\mu_3\text{-}O)_2(CH_3COO)_4(L1)_4]^-$ and $[Mn^{III}_5(\mu_3\text{-}O)_2(CH_3COO)_4(L2)_4]^-$ have been synthesised by using two Schiff base ligands derived from 3,5-diamino-1,2,4-triazole, following two different preparative routes, either using the pre-formed ligand (for L1) or *via* a metal-mediated template synthesis (for L2). The $\{Mn^{III}_5\}$ structure is unusual, being based on two corner-sharing perpendicular $\{Mn_3\}$ triangles forming a twisted bow-tie. The magnetic studies reveal antiferromagnetic coupling between Mn(III) ions while electrochemical experiments are consistent with a quasi-reversible Mn(III)↔Mn(IV) redox process at the central manganese ion.

Introduction

Manganese is an excellent candidate for the synthesis and study of new molecular magnetic materials[1–5] with a range of easily accessible oxidation states from Mn(II) to Mn(IV).[6–8] Mn(III) ions are employed in the design of nanomagnets due to the characteristic magnetic anisotropy (D),[9–12] whereas Mn(II) ions are used in molecular magnetic refrigerants, considering the relatively large number of unpaired electrons and the typical isotropic octahedral environment.[13,14] In addition, the stability of these multiple oxidation states provides an opportunity to explore the redox properties in polymetallic Mn complexes.[15–17] The synthetic routes to these complexes are mainly serendipitous self-assembly, which commonly uses flexible ligands, and/or rational design, which involves more rigid, polycompartmental ligands.[18–20] One of the advantages of the second approach is the degree of control in the assembly of the metal ions through the pre-design of the ligand. Schiff base ligands have been used in this type of strategy,[20–22] and in some cases, these ligands can provide additional redox properties to complexes as a result of the presence of iminic groups.[23] Importantly, the iminic bonds make the ligand flexible enough to accommodate different coordination environments based on the type and/or valence of the metal ions. Considering these factors, we proposed the use of the 3,5-diamino-1,2,4-triazole derivatives, *N*-(2-hydroxy-3-methoxybenzylene)-3,5-diamino-1,2,4-triazole (H_2L1) and *N*-salycilene-3,5-diamino-1,2,4-triazole (H_2L2) to direct the synthesis of new polymetallic manganese complexes. Unlike other diamines, 3,5-diamino-1,2,4-triazole derivatives have not been explored in the synthesis, magnetic and electrochemical studies of high-nuclearity complexes. Herein we describe two different synthetic methodologies for the preparation of two new pentanuclear Mn(III) compounds, $(HNEt_3)[Mn^{III}_5(\mu_3\text{-}O)_2(CH_3COO)_4(L1)_4]\cdot 4CH_3CN\cdot 4H_2O$ (**1**) and $(HNEt_3)[Mn^{III}_5(\mu_3\text{-}O)_2(CH_3COO)_4(L2)_4]\cdot CH_3CN\cdot 2CH_3OH$ (**2**) and report their structural, magnetic and electrochemical properties.

Experimental section

Materials and physical measurements

All reagents and solvents were obtained from commercial suppliers and used without further purification.

Crystallographic data were collected for **1** and **2** at 100 K using Mo-Kα radiation (λ = 0.71073 Å). For **1** a Bruker APEXII CCD diffractometer with an Oxford Cryosystems n-Helix low-temperature device mounted on a sealed tube generator was used; for **2** a Rigaku AFC12 goniometer equipped with an (HG) Saturn724+ detector mounted on an FR-E+ SuperBright rotating anode generator with HF Varimax optics (100 μm focus).[24] Both structures were solved using SHELXT[25] and refined using

[a]*WestChem, School of Chemistry, University of Glasgow, University Avenue, Glasgow, G12 8QQ, UK. E-mail: mark.murrie@glasgow.ac.uk*
[b]*Graduate School of Pure and Applied Sciences, University of Tsukuba, Tennodai 1-1-1, Tsukuba 305-8571, Japan*

†Electronic supplementary information (ESI) available: Crystallographic data, structure and detail of the crystal structure of **1** and **2**, table with bond valence sum calculations, powder X-ray diffraction (PXRD) pattern of **1**, further magnetic data and cyclic voltammetry of ligand H_2L1. CCDC 1519689 and 1519690. For ESI and crystallographic data in CIF or other electronic format see DOI: 10.1039/c7dt02430d

‡Current address: Institute for Integrated Cell-Material Science (WPI-iCeMS), Kyoto University, Yoshida, Sakyo-ku, Kyoto 606-8501, Japan.

full-matrix least squares refinement on F^2 using SHELX2014[26] within OLEX2.[27] SQUEEZE was used to calculate and account for diffuse solvent in **2**.[28] Further details of disorder modelling and hydrogen atom treatment are given in the ESI.† The powder X-ray patterns for **1** and **2** were collected on a PANalytical XPert MPD, with Cu Kα1 radiation at ambient temperature over a range of $5° < 2\theta < 50°$ using a step size of 0.0167°. The calculated pattern was generated from Mercury using the .cif of the crystal structure at 100 K.

The IR spectra were measured using a FTIR-8400S SHIMADZU IR spectrophotometer. The microanalyses and mass spectrometry analyses were performed by the analytical services of the School of Chemistry at the University of Glasgow. The ^{1}H-NMR spectrum of H_2L1 was obtained using a Bruker AVI 400 M MHz. Magnetic measurements of complexes **1** and **2** were carried out on phase-pure (Fig. S4 in the ESI†) polycrystalline samples that were lightly powdered and constrained in eicosane, using a Quantum Design MPMS-XL SQUID magnetometer. Data were corrected for the diamagnetic contribution of the sample holder and eicosane by measurements, and for the diamagnetism of the compounds. Electrochemical measurements were performed on a CH Instruments 760D Electrochemical Workstation using CHI Version 10.03 software. Electrochemical experiments for obtaining the cyclic voltammograms (CVs) were conducted at 298 K using a CH Instruments glassy carbon button working electrode (area = 0.071 cm^2), BASi Ag/AgNO$_3$ pseudo reference electrode, and Pt mesh counter electrode in a single compartment cell. Bulk electrolyses were performed in a similar manner, but using a large surface area reticulated glassy carbon electrode (BASi) as the working electrode. All electrode potentials were referenced to the ferrocene/ferrocenium couple by doping in samples of ferrocene to the electrolyte, and all potentials given in this work are reported relative to the ferrocene/ferrocenium couple. All electrochemical experiments were conducted in electrolyte solutions prepared using dry *N*,*N*-dimethylformamide (DMF), and were thoroughly degassed with argon. The supporting electrolyte was tetrabutylammonium hexafluorophosphate at a concentration of 0.2 mol dm^{-3}. Solutions were agitated between acquisition of individual CVs and CVs were corrected for resistance, using the *iR* compensation function of the potentiostat. CVs were collected from unstirred solutions and bulk electrolyses were undertaken in stirred solutions.

Synthetic methods

$C_{10}H_{11}N_5O_2$ (H_2L1). To a suspension of 3,5-diamino-1,2,4-triazole (0.85 g, 8.6 mmol) in CH_3OH (115 mL) *o*-vanillin (1.31 g, 8.6 mmol) was added. The resultant yellow solution was stirred and refluxed for 5 hours to yield a deep yellow suspension. Once cooled, the final yellow precipitate was collected *via* filtration, washed with small volumes of MeOH and dried with Et_2O. Yield 83% (1.67 g). ^{1}H-NMR (DMSO-d$_6$): 3.83 (s; 3H, CH_3), 6.23 (s; 2H, NH_2), 6.91 (t, 1H, C_{Ar}–H), 7.14 (d, 1H, C_{Ar}–H), 7.26 (d, 1H, C_{Ar}–H), 9.15 (s; 1H, HC=N), 12.13 (s; 1H, OH), 12.87 (s; 1H, NH). IR ($\bar{\nu}$ in cm^{-1}): 3127 (m), 1651 (s), 1605 (s), 1469 (m) 1256 (s), 970 (s), 785 (s), 735 (s). MS (ESI+, *m*/*z*): 256 $[C_{10}H_{11}N_5O_2 + Na]^+$.

$(HNEt_3)[Mn^{III}_5(\mu_3\text{-}O)_2(CH_3COO)_4(L1)_4]\cdot 4CH_3CN\cdot 4H_2O$ (1). $Mn(CH_3COO)_3\cdot 2H_2O$ (0.1 g, 0.37 mmol) was added to a pale yellow suspension of H_2L1 (0.07 g, 0.3 mmol) in CH_3CN (20 mL) to give a pale brown suspension. A solution of Et_3N (0.08 mL, 0.6 mmol) was then added drop-wise to give a dark brown suspension. The suspension was then heated to 90 °C for one and a half hours after which a dark brown solution was attained. Dark brown plate-like single crystals suitable for X-ray diffraction were obtained after 4 days through slow evaporation. Yield 48% (53 mg). IR ($\bar{\nu}$ in cm^{-1}): 3385 (w), 1584 (s), 1431 (s), 1250 (s), 1215 (s), 974 (w), 746 (m), 606 (s). Elemental analysis: $((HNEt_3)[Mn^{III}_5(\mu_3\text{-}O)_2(CH_3COO)_4(L1)_4]\cdot 5H_2O)$ [%], found: C 39.68, H 4.34, N 17.58; calc.: C 39.10, H 4.44, N 17.73. MS (ESI−, CH_3CN, *m*/*z*): 1469 $[M]^-$. MS (ESI+, DMF, *m*/*z*): 1429 $[M - OAc + H_3O]^+$.

$(HNEt_3)[Mn^{III}_5(\mu_3\text{-}O)_2(CH_3COO)_4(L2)_4]\cdot CH_3CN\cdot 2CH_3OH$ (2). A solution of salicylaldehyde (0.13 mL, 1.25 mmol) was added to a suspension of 3,5-diamino-1,2,4-triazole (0.12 g, 1.25 mmol) in CH_3OH (50 mL). To the resulting pale yellow solution a light brown suspension of $Mn(CH_3COO)_3\cdot 2H_2O$ (0.42 g, 1.56 mmol) in CH_3CN (50 mL) was added to give a dark brown suspension. Et_3N (0.35 ml, 2.50 mmol) and $Na(CH_3COO)$ (0.10 g, 1.25 mmol) were consecutively added, giving a dark green-brown suspension. The suspension was heated at 90 °C for one and a half hours. Dark brown plate-like single crystals suitable for X-ray diffraction appeared after 3 days through slow evaporation of the reaction solution. Yield 31% (131 mg). IR ($\bar{\nu}$ in cm^{-1}): 3389 (w), 1585 (s), 1441 (m), 1404 (m), 1288 (s), 924 (m), 760 (s), 604 (s). Elemental analysis: $((HNEt_3)[Mn^{III}_5(\mu_3\text{-}O)_2(CH_3COO)_4(L2)_4]\cdot 1.75CH_3OH\cdot 5H_2O)$ [%], found: C 38.78, H 4.37, N 18.29; calc.: C 38.97, H 4.55, N 18.44. MS (ESI+, CH_3CN, *m*/*z*): 1372 $[M + H + Na]^+$.

Results and discussion

There are very few examples of complexes formed using 1,2,4-triazole derivatives where the magnetic properties have been investigated, these being mainly copper complexes.[29–33] Surprisingly, there is a lack of magnetic studies performed on such complexes with other 3d ions (*vide supra*) such as Mn. Furthermore, the only report of the coordination chemistry of L1 and L2 is with oxovanadium(IV).[34] H_2L1 was prepared from the condensation reaction between 3,5-diamino-1,2,4-triazole and 2-hydroxy-3-methoxy-benzaldehyde (*o*-vanillin) in methanol. The synthetic route to H_2L1 (Scheme 1) is simplified compared to that previously reported,[34] as we obtained pure H_2L1 straight from the condensation without re-crystallisation (checked by ^{1}H NMR).[34]

The reaction between H_2L1 and $Mn(CH_3COO)_2\cdot 4H_2O$ in the presence of Et_3N allows the assembly of $(HNEt_3)$-$[Mn^{III}_5(\mu_3\text{-}O)_2(CH_3COO)_4(L1)_4]\cdot 4CH_3CN\cdot 4H_2O$ (**1**). An alternative synthetic route to that described for H_2L1 was carried out to obtain H_2L2 (see Fig. 1, left), based on the use of salicylaldehyde

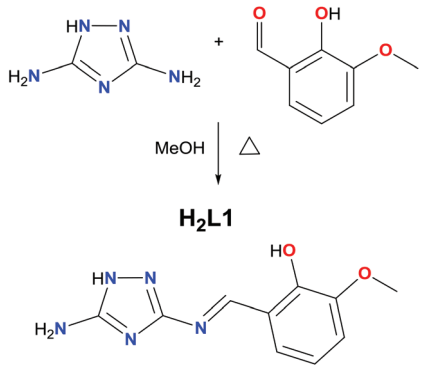

Scheme 1 The ligand *N*-(2-hydroxy-3-methoxybenzylene)-3,5-diamino-1,2,4-triazole (H_2L1).

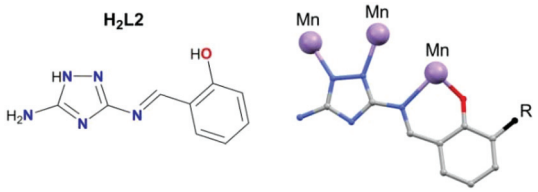

Fig. 1 Ligand H_2L2 (left), and general coordination mode of the deprotonated ligands (right). R = OCH_3 for H_2L1, and R = H for H_2L2.

instead of *o*-vanillin. The condensation reaction to form the Schiff base was avoided as we were not able to isolate H_2L2 as a pure product. Instead, a metal mediated template synthesis was used, yielding successfully the isostructural complex $(HNEt_3)[Mn_5^{III}(\mu_3\text{-}O)_2(CH_3COO)_4(L2)_4]\cdot CH_3CN\cdot 2CH_3OH$ (**2**).[35,36] Note that our attempts to form coordination complexes using the corresponding di-substituted 1,2,4-triazole ligands proved unsuccessful, and in the case of the reaction with $Mn(CH_3COO)_2\cdot 4H_2O$ the di-substituted ligand decomposed through breaking one imine bond to coordinate as H_2L1 or H_2L2.

X-ray crystallographic analysis

Selected crystallographic experimental details for **1** and **2** are shown in Table S1.† Both complexes crystallise in the monoclinic space group $P2_1/n$. The asymmetric unit of **1** and **2** contains one $[Mn_5^{III}(\mu_3\text{-}O)_2(CH_3COO)_4(L1)_4]^-$ anion (**1**) or $[Mn_5^{III}(\mu_3\text{-}O)_2(CH_3COO)_4(L2)_4]^-$ anion (**2**), one $HNEt_3^+$ cation, and several solvent molecules (four water and four acetonitrile molecules for **1**; one acetonitrile and two methanol molecules for **2**). Note that for **2** a poorly defined solvent region was additionally treated using SQUEEZE.[28] The solvent accessible voids were calculated to be 190 Å^3 containing 42 electrons per complex which can be attributed to 4 molecules of H_2O, given the results from the elemental analysis. As both anionic complexes are isostructural, the following description is valid for **1** and **2** (see structure in Fig. S1 of the ESI†). The structure of **1** involves five Mn(III) ions arranged within two fused $\{Mn_3O\}$ units which share a central Mn(III) ion (Fig. 2). The oxidation

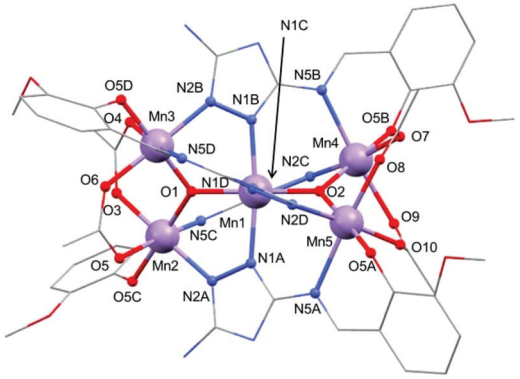

Fig. 2 Structure of the anionic complex in **1**. C, grey; Mn, lavender; N, blue; O, red; only Mn and N, O atoms involved in the coordination of the Mn centres are labelled. Hydrogen atoms and solvent molecules are omitted for clarity.

state of each manganese centre has been confirmed by bond length and charge balance considerations, and also by bond valence sum calculations (BVS) with values presented in Table S2.†[37] The two corner-sharing $\{Mn_3O\}$ units lie in planes almost perpendicular to one another with angles of 86.84° (**1**) and 86.75° (**2**) (see Fig. S2 of the ESI†). Each Mn(III) center displays a tetragonally distorted octahedral geometry through the coordination of four doubly deprotonated Schiff base ligands ($L1^{2-}$ for **1**, and $L2^{2-}$ for **2**) and four bidentate acetate auxiliary ligands (see Fig. 2). Two different Mn(III) ions can be distinguished based on the dissimilarities of their first coordination sphere (see Fig. 2 and Fig. S1 of the ESI†). The central Mn1 shared by the two fused $\{Mn_3O\}$ units is surrounded by four ligand units ($L1^{2-}$ for **1**, and $L2^{2-}$ for **2**) through the coordination of four N-donor atoms from the triazole rings. Moreover, two μ_3-oxo bridges (O1, O2) fill the remaining equatorial positions of Mn1. These oxo groups also connect the central Mn1 ion with the outer manganese ions (Mn2, Mn3, Mn4, Mn5) with average Mn–O bond distances of 1.885(2) Å for **1** and 1.887(5) Å for **2**. Each outer Mn(III) ion is further coordinated by one phenolic oxygen and two N atoms, a nitrogen from the triazole ring of one ligand and the iminic nitrogen of another. Two bidentate acetate anions are additionally bound which link each ion to the adjacent peripheral Mn(III) (see Fig. 2). The intramolecular Mn···Mn′ distances can be divided in two groups: those between the central manganese atom Mn1 and the peripheral ones Mn2–Mn5 ($d^{Avg}_{Mn1\cdots Mn'}$ = 3.252(8) Å for **1**, and 3.253(1) Å for **2**), and those between the outer Mn(III) ions linked by the acetate groups (3.291(7) Å for **1**, and 3.300(1) Å for **2**).

The outer manganese centres (Mn2–Mn5) in **1** and **2** display a characteristic elongated Jahn–Teller (JT) distortion (Fig. 3), as expected for high-spin d^4 Mn(III) ions (d^{Avg}_{Mn-N} = 2.298 Å (**1**), 2.283 Å (**2**); d^{Avg}_{Mn-N} = 2.035 Å (**1**), 2.032 Å (**2**)). The elongated JT axis around the central manganese (Mn1) however is comparatively less distinct. This is evident on considering the bond lengths around Mn2–Mn5 as internal standards, and comparing these to those of Mn1. The Mn1–N

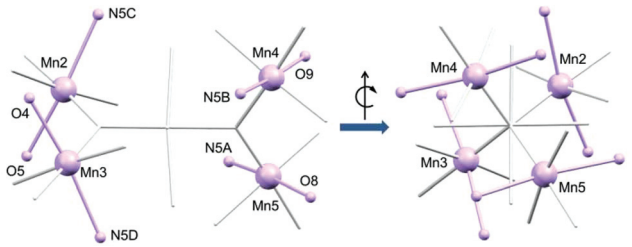

Fig. 3 Detail of the metal core of **1**. Only O, N, and metal ions involved in the Jahn–Teller (JT) axes of Mn2–Mn5 are labelled. JT axes are highlighted in lavender.

distances (N1A–Mn1–N1B) are shorter than expected (2.162 Å (**1**), 2.158 Å (**2**)) and the Mn1–N distances (N1C–Mn1–N1D) are slightly longer than would be expected (2.096 Å (**1**), 2.074 Å (**2**)) compared to those of the outer Mn(III) ions. This indicates possible disorder of the JT axis between these two positions.[38] Note, the Mn1–O1 and Mn–O2 distances are as expected on comparison to the other Mn–O distances not situated along the JT axes of Mn2–Mn5. We have therefore assumed the axis defined by O1–Mn1–O2 is not involved in the disorder.

An extensive search of the Cambridge Structural Database (CSD 5.38, June 2017) reveals the rarity of the metal-oxo assembly displayed for **1** and **2**, as only five structures displaying a similar $\{M_5O_2\}$ topology are reported (M being Mn, Fe, Co, Ni or Zn, and the bridging ligand an oxo or hydroxo group).[39–41] It is important to stress that only one of the published structures is formed by Mn ions $([Mn_4^{III}Mn^{II}Na_2O_2(O_2CMe)_4(L')_4(DMF)_4(H_2O)]$, where H_2L' = 2-hydroxyphenyl-1,3,4-oxadiazole-2(3*H*)-thione).[41] Therefore, the topology displayed by **1** and **2** is quite unusual for manganese-based polymetallic complexes, especially compared with more common metal arrangements for Mn(II/III) ions, such as a butterfly-like assembly.[5,42,43]

Magnetic properties

Variable-temperature magnetic susceptibility data were measured in an applied field of 1000 Oe in the range of 290 to 2 K (see Fig. 4). Variable-field magnetisation measurements were also carried out between 0 and 5 T at 2, 4 and 6 K for each complex (Fig. S6†). At 290 K the experimental $\chi_M T$ values observed for **1** and **2** (11.5 $cm^3\ mol^{-1}$ K and 11.9 $cm^3\ mol^{-1}$ K respectively) are lower than the theoretical spin-only value for five non-interacting Mn(III) ions (15.0 $cm^3\ mol^{-1}$ K, considering S = 2, and g = 2). Below 290 K, the $\chi_M T$ value decreases, reaching a minimum value of 0.79 $cm^3\ mol^{-1}$ K for **1** and 0.80 $cm^3\ mol^{-1}$ K for **2** at 2 K, consistent with predominant intramolecular antiferromagnetic interactions. The susceptibility data for **1** and **2** were fitted using the program Phi,[44] considering the magnetic model shown in Fig. 4 (inset) and the spin Hamiltonian shown below (eqn (1)).

Initially zero-field splitting (ZFS) was not included to avoid over-parameterisation. Two different exchange interactions were considered for complexes **1** and **2** (see magnetic model above) – that between the central Mn1 and each of the outer-lying manganese centres ($\mathcal{J}_1$) and the interaction between the

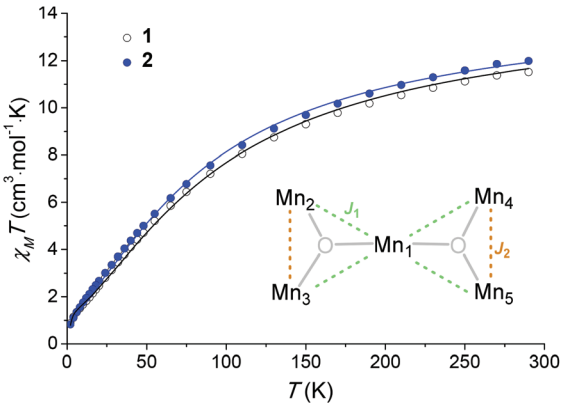

Fig. 4 Temperature dependence of $\chi_M T$ for **1** (shown in white) and **2** (blue). The inset shows the topology of the intramolecular magnetic interactions considered to fit **1** and **2** (see text for details). The solid lines correspond to the fit of the data.

Mn(III) centres of each peripheral pair ($\mathcal{J}_2$). The g parameter was included as a fixed value of g = 1.98.[45–47] The best fit gives the coupling constants $\mathcal{J}_1 = -3.10\ cm^{-1}$ (**1**), $-2.82\ cm^{-1}$ (**2**), and $\mathcal{J}_2 = -8.26\ cm^{-1}$ (**1**), $-7.43\ cm^{-1}$ (**2**) (R = 98% and 95%). Antiferromagnetic interactions are also seen in a mixed-valence $\{Mn_4^{III}Mn^{II}\}$ complex with a related structure ($\mathcal{J}_1 = -1.15\ cm^{-1}$ and $\mathcal{J}_2 = -2.40\ cm^{-1}$).[41] Given the magnitude of the exchange interactions it is clear that axial zero-field splitting (D) should also be included, as this can be of the same order of magnitude as $\mathcal{J}$.[3] However all attempts to include D lead to unreasonable values and/or prevent the fits from converging.

$$\hat{H} = -2\mathcal{J}_1\left(\hat{S}_1\hat{S}_2 + \hat{S}_1\hat{S}_3 + \hat{S}_1\hat{S}_4 + \hat{S}_1\hat{S}_5\right) - 2\mathcal{J}_2\left(\hat{S}_2\hat{S}_3 + \hat{S}_4\hat{S}_5\right) + g\mu_B\vec{B}\sum_{i=1}^{5}\vec{s}_i \quad (1)$$

The simple exchange-coupling model which ignores ZFS suggests that the ground state of both **1** and **2** is S = 0 with low-lying excited states: the closest lying S = 1 state within 3 cm^{-1} and the closest lying S = 2 state within 6 cm^{-1} (Fig. S5†). The magnetisation curves (Fig. S6†) would then result from population of these low-lying S > 0 states. Note that inclusion of single-ion ZFS in the model (*vide supra*) could modify the obtained $\mathcal{J}$ values and hence the ordering of the spin states, which may reveal a non-zero ground state. Additional alternating-current (ac) measurements were performed, with the absence of any frequency-dependent out-of-phase signal (Fig. S7†) consistent with either an S = 0 ground state or a small spin ground state with a negligible D parameter. Note that the Jahn–Teller axes of the four outer manganese ions are nearly perpendicular to each other (Fig. 3), which would yield a relatively small net axial magnetic anisotropy.[48]

Electrochemical studies

Along with the redox properties of the metal ions, Schiff base ligands can potentially impart intriguing redox activity to their

complexes, as a result of the presence of iminic groups.[49] The redox behavior of complexes **1** and **2** was therefore probed by cyclic voltammetry (CV). Fig. 5a shows the CV of compound **2** over the range +1 to −2.5 V *vs.* the ferrocene/ferrocenium couple (the CV of complex **1** over the same range is very similar). A CV of ligand H_2L1 is provided in the ESI (Fig. S8†) for comparison. Fig. 5a indicates that at least two essentially irreversible reductive redox processes that cannot be attributed to the free ligand are evident at around −0.9 V and −1.8 V. These reductive waves did not become more reversible when the scan window was restricted. However, in the oxidative portion of the voltammogram, a more reversible wave (centred around +0.25 V) was apparent. Fig. 5b shows a comparison of the CVs for this oxidative process for complexes **1** and **2** over a smaller potential window than in Fig. 5a. Again, the free ligand shows no redox waves in this region (Fig. S8†). The shape profile was very similar in both cases, and $E_{1/2}$ values of 0.21 V and 0.23 V were obtained for complexes **1** and **2** respectively (these values are the same within the ±20 mV error quoted for the type of $Ag/AgNO_3$ pseudo reference employed). Taken together, and in view of the structural similarities between complexes **1** and **2**, these data suggest that the redox process giving rise to this wave has the same origin in both complexes.

Bulk electrolysis on complex **1** at +0.47 V indicated that the charge passed during this oxidation process was equal to 95% of that expected for a one-electron process. It is therefore plausible that this redox process corresponds to the one-electron oxidation and re-reduction of the unique, central Mn(III) centre Mn1 in these complexes given the different coordination environment displayed – $\{MnN_4O_2\}$ – compared to Mn2–5 – $\{MnN_2O_4\}$. The kinetics of the redox process giving rise to the wave at +0.21 V for complex **1** were probed by scan-rate dependency studies. As is evident from Fig. 6, the return (cathodic) peak currents are always smaller than the oxidative currents, with this effect becoming less apparent as the scan rate is increased (*i.e.* the wave becomes more reversible the shorter the length of time the compound remains oxidised). This is consistent with an oxidation process followed by an irreversible chemical decomposition. Thus at fast scan rates, there is a greater chance that the complex can be reduced back to its original form before decomposition can occur. Moreover, Fig. 6 shows that even at slow scan-rates, the peak-to-peak separation is well over 100 mV, indicating that electron transfer is rather slow. This could imply that a structural re-arrangement occurs during this redox event and the associated geometrical changes required around a Mn(III) centre upon oxidation to Mn(IV) (and upon re-reduction to Mn(III)) could account for the slow electron transfer observed. It is interesting to note that the crystallographic analysis indicates possible disorder of the Jahn–Teller axis at the central Mn(III), which may make the redox event easier at this site.

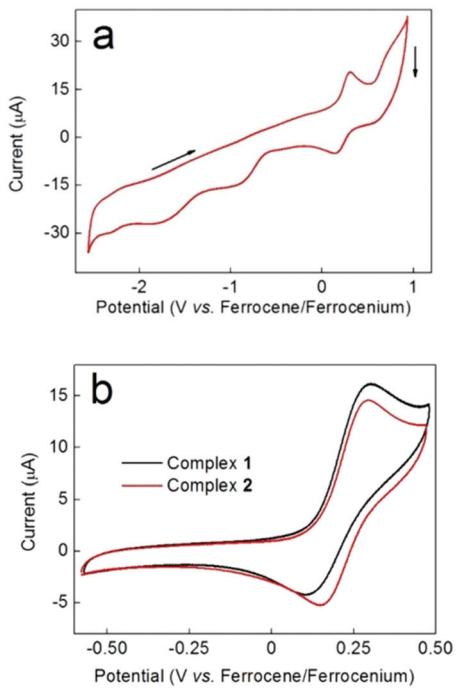

Fig. 5 (a) CV of a 2 mM solution of complex **2** at a scan rate of 100 mV s^{-1} over the range +1 to −2.5 V *vs.* ferrocene/ferrocenium. (b) Comparison between CVs of 2 mM solutions of complexes **1** and **2**, both at a scan rate of 100 mV s^{-1} over a narrower potential window.

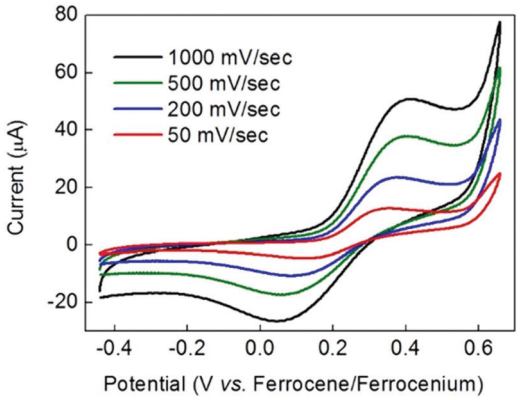

Fig. 6 Comparison between CVs of a 4 mM solution of complex **1** at various scan rates as indicated.

Conclusions

We have shown for the first time that the 1,2,4-triazole derivatives H_2L1 and H_2L2 can be utilised in the synthesis of polymetallic transition complexes. This leads to two novel pentanuclear Mn(III)-based complexes with an unusual twisted bow-tie structure, where the Mn(III) ions are antiferromagnetically coupled. The electrochemical studies reveal a quasi-reversible redox process: a one-electron oxidation Mn(III) → Mn(IV) and re-reduction Mn(IV) → Mn(III) which we suggest to be centred at the central Mn(III) ion in both complexes. Future work will focus on modifying the Schiff base ligands to impart

additional redox states towards redox-switchable molecular magnetic materials.

Conflicts of interest

There are no conflicts to declare.

Acknowledgements

The data which underpin this work are available at DOI: 10.5525/gla.researchdata.444. M. H. O. is thankful to the Japan Society for the Promotion of Science (JSPS) for the Short Term Pre/Postdoctoral Fellowship for International Research. We thank the EPSRC UK National Crystallographic Service for single crystal data collection. CCDC 1519689 and 1519690 contain the supplementary crystallographic data for this paper.†

Notes and references

1 G. Rajaraman, M. Murugesu, E. C. Sañudo, M. Soler, W. Wernsdorfer, M. Helliwell, C. Muryn, J. Raftery, S. J. Teat, G. Christou and E. K. Brechin, *J. Am. Chem. Soc.*, 2004, **126**, 15445–15457.
2 V. A. Milway, F. Tuna, A. R. Farrell, L. E. Sharp, S. Parsons and M. Murrie, *Angew. Chem., Int. Ed.*, 2013, **52**, 1949–1952.
3 G. A. Craig, J. J. Marbey, S. Hill, O. Roubeau, S. Parsons and M. Murrie, *Inorg. Chem.*, 2015, **54**, 13–15.
4 C.-I. Yang, W. Wernsdorfer, G.-H. Lee and H.-L. Tsai, *J. Am. Chem. Soc.*, 2007, **129**, 456–457.
5 G. E. Kostakis, A. M. Ako and A. K. Powell, *Chem. Soc. Rev.*, 2010, **39**, 2238–2271.
6 T. Lis, *Acta Crystallogr., Sect. B: Struct. Crystallogr. Cryst. Chem.*, 1980, **36**, 2042–2046.
7 R. Sessoli, H. L. Tsai, A. R. Schake, S. Wang, J. B. Vincent, K. Folting, D. Gatteschi, G. Christou and D. N. Hendrickson, *J. Am. Chem. Soc.*, 1993, **115**, 1804–1816.
8 R. Sessoli, D. Gatteschi, A. Caneschi and M. A. Novak, *Nature*, 1993, **365**, 141–143.
9 G. A. Craig and M. Murrie, *Chem. Soc. Rev.*, 2015, **44**, 2135–2147.
10 K. S. Pedersen, J. Bendix and R. Clerac, *Chem. Commun.*, 2014, **50**, 4396–4415.
11 P. L. Feng, C. Koo, J. J. Henderson, P. Manning, M. Nakano, E. del Barco, S. Hill and D. N. Hendrickson, *Inorg. Chem.*, 2009, **48**, 3480–3492.
12 P. Parois, S. A. Moggach, J. Sanchez-Benitez, K. V. Kamenev, A. R. Lennie, J. E. Warren, E. K. Brechin, S. Parsons and M. Murrie, *Chem. Commun.*, 2010, **46**, 1881–1883.
13 M. Manoli, A. Collins, S. Parsons, A. Candini, M. Evangelisti and E. K. Brechin, *J. Am. Chem. Soc.*, 2008, **130**, 11129–11139.
14 G. Karotsis, S. Kennedy, S. J. Teat, C. M. Beavers, D. A. Fowler, J. J. Morales, M. Evangelisti, S. J. Dalgarno and E. K. Brechin, *J. Am. Chem. Soc.*, 2010, **132**, 12983–12990.
15 H. Y. V. Ching, E. Anxolabehere-Mallart, H. E. Colmer, C. Costentin, P. Dorlet, T. A. Jackson, C. Policar and M. Robert, *Chem. Sci.*, 2014, **5**, 2304–2310.
16 D. Shevchenko, P. Huang, V. V. Bon, M. F. Anderlund, V. N. Kokozay, S. Styring and A. Thapper, *Dalton Trans.*, 2013, **42**, 5130–5139.
17 H. Sato, M. Yamaguchi, T. Onuki, M. Noguchi, G. N. Newton, T. Shiga and H. Oshio, *Eur. J. Inorg. Chem.*, 2015, 2193–2198.
18 R. E. P. Winpenny, *J. Chem. Soc., Dalton Trans.*, 2002, 1–10.
19 R. W. Saalfrank, H. Maid and A. Scheurer, *Angew. Chem., Int. Ed.*, 2008, **47**, 8794–8824.
20 T. Glaser, *Chem. Commun.*, 2011, **47**, 116–130.
21 E. Colacio, J. Ruiz-Sanchez, F. J. White and E. K. Brechin, *Inorg. Chem.*, 2011, **50**, 7268–7273.
22 S. G. Dogaheh, M. Heras Ojea, L. R. Piquer, L. Artús Suàrez, H. Khanmohammadi, G. Aromí and E. C. Sañudo, *Eur. J. Inorg. Chem.*, 2016, **20**, 3314–3321.
23 T. J. Dunn, C. F. Ramogida, C. Simmonds, A. Paterson, E. W. Y. Wong, L. Chiang, Y. Shimazaki and T. Storr, *Inorg. Chem.*, 2011, **50**, 6746–6755.
24 S. J. Coles and P. A. Gale, *Chem. Sci.*, 2012, **3**, 683–689.
25 G. Sheldrick, *Acta Crystallogr., Sect. A: Fundam. Crystallogr.*, 2008, **64**, 112–122.
26 G. Sheldrick, *Acta Crystallogr., Sect. C: Cryst. Struct. Commun.*, 2015, **71**, 3–8.
27 O. V. Dolomanov, L. J. Bourhis, R. J. Gildea, J. A. K. Howard and H. Puschmann, *J. Appl. Crystallogr.*, 2009, **42**, 339–341.
28 A. Spek, *J. Appl. Crystallogr.*, 2003, **36**, 7–13.
29 S. Ferrer, P. J. van Koningsbruggen, J. G. Haasnoot, J. Reedijk, H. Kooijman, A. L. Spek, L. Lezama, A. M. Arif and J. S. Miller, *J. Chem. Soc., Dalton Trans.*, 1999, 4269–4276.
30 S. Ferrer, J. G. Haasnoot, J. Reedijk, E. Müller, M. Biagini Cingi, M. Lanfranchi, A. M. Manotti Lanfredi and J. Ribas, *Inorg. Chem.*, 2000, **39**, 1859–1867.
31 S. Ferrer, E. Aznar, F. Lloret, A. Castiñeiras, M. Liu-González and J. Borrás, *Inorg. Chem.*, 2007, **46**, 372–374.
32 S. Ferrer, F. Lloret, E. Pardo, J. M. Clemente-Juan, M. Liu-González and S. García-Granda, *Inorg. Chem.*, 2012, **51**, 985–1001.
33 J. Hernández-Gil, N. Ovèjak, S. Ferrer, F. Lloret and A. Castiñeiras, *Inorg. Chem.*, 2013, **52**, 2289–2291.
34 S. H. Sumrra and Z. H. Chohan, *J. Enzyme Inhib. Med. Chem.*, 2013, **28**, 1291–1299.
35 P. A. Vigato and S. Tamburini, *Coord. Chem. Rev.*, 2004, **248**, 1717–2128.
36 M. Andruh, *Chem. Commun.*, 2011, **47**, 3025–3042.
37 I. D. Brown and K. K. Wu, *Acta Crystallogr., Sect. B: Struct. Crystallogr. Cryst. Chem.*, 1976, **32**, 1957–1959.

38 C. Murray, B. Gildea, H. Muller-Bunz, C. J. Harding and G. G. Morgan, *Dalton Trans.*, 2012, **41**, 14487–14489.
39 J. Tabernor, L. F. Jones, S. L. Heath, C. Muryn, G. Aromi, J. Ribas, E. K. Brechin and D. Collison, *Dalton Trans.*, 2004, 975–976.
40 Y. Wei, H. Hou, Y. Fan and Y. Zhu, *Eur. J. Inorg. Chem.*, 2004, **19**, 3946–3957.
41 C. Beghidja, G. Rogez and R. Welter, *New J. Chem.*, 2007, **31**, 1403–1406.
42 J. Yoo, E. K. Brechin, A. Yamaguchi, M. Nakano, J. C. Huffman, A. L. Maniero, L.-C. Brunel, K. Awaga, H. Ishimoto, G. Christou and D. N. Hendrickson, *Inorg. Chem.*, 2000, **39**, 3615–3623.
43 R. McLellan, M. A. Palacios, E. K. Brechin and S. J. Dalgarno, *ChemPlusChem*, 2014, **79**, 667–670.
44 N. F. Chilton, R. P. Anderson, L. D. Turner, A. Soncini and K. S. Murray, *J. Comput. Chem.*, 2013, **34**, 1164–1175.
45 G. Aromí, P. Gamez, O. Roubeau, P. C. Berzal, H. Kooijman, A. L. Spek, W. L. Driessen and J. Reedijk, *Inorg. Chem.*, 2002, **41**, 3673–3683.
46 A. Konstantatos, R. Bewley, A.-L. Barra, J. Bendix, S. Piligkos and H. Weihe, *Inorg. Chem.*, 2016, **55**, 10377–10382.
47 C. J. Milios, A. Prescimone, A. Mishra, S. Parsons, W. Wernsdorfer, G. Christou, S. P. Perlepes and E. K. Brechin, *Chem. Commun.*, 2007, 153–155.
48 A. Ferguson, K. Thomson, A. Parkin, P. Cooper, C. J. Milios, E. K. Brechin and M. Murrie, *Dalton Trans.*, 2007, 728–730.
49 E. Castillo-Martínez, J. Carretero-González and M. Armand, *Angew. Chem., Int. Ed.*, 2014, **53**, 5341–5345.